Tetrahedron 66 (2010) 845–851

Contents lists available at ScienceDirect

Tetrahedron

journal homepage: www.elsevier.com/locate/tet

Formation and sigmatropic rearrangement of $PhCOC(NO_2)=CH_2$ cycloadducts of 1,3-cyclohexadiene: a theoretical study

Hanying Xu [a,*], Peter A. Wade [b,*], Karl Sohlberg [b]

[a] Department of Physical Sciences, Kingsborough Community College, 2001 Oriental Blvd., Brooklyn, NY 11235, USA
[b] Department of Chemistry, Drexel University, Philadelphia, PA 19104, USA

ARTICLE INFO

Article history:
Received 2 July 2009
Received in revised form
16 November 2009
Accepted 17 November 2009
Available online 20 November 2009

ABSTRACT

Competing cycloaddition pathways for the reaction of 2-nitro-1-phenyl-2-propen-1-one with 1,3-cyclohexadiene were investigated employing computational methods. A bifurcating pathway was found for formation of nitroketone **3** and nitronic ester **5**. A second bifurcating pathway was found for the formation of nitroketone **4** and enol ether **6**. Sigmatropic rearrangements of two cycloadducts, nitronic ester **5** and enol ether **6**, were also studied computationally. The reaction pathways were mapped using the B3-LYP/6-311G(d) method and relative energies for species **3**–**6** were calculated at the same level. Solution-phase corrections were performed by the PCM method. The calculations for both bifurcating cycloaddition pathways indicate kinetic control with similar rate-determining activation energies. The nitroketone **3** is more stable than nitronic ester **5** by 5.3 kcal/mol and nitroketone **4** is more stable than enol ether **6** by 3.9 kcal/mol, consistent with the observed direction of sigmatropic rearrangement.

© 2009 Elsevier Ltd. All rights reserved.

1. Introduction

Four isomeric cycloaddition products were previously reported from the reaction of 2-nitro-1-phenyl-2-propen-1-one with 1,3-cyclohexadiene (**2**) (Scheme 1).[1] Nitroketone **1** functions as a Diels–Alder dienophile affording the diastereomeric bridged bicyclic nitroketones **3** (*endo*-nitro) and **4** (*exo*-nitro), respectively, in 20% and 21% yield. In two additional competing pathways, nitroketone **1** functions as the diene. It serves as a 1-oxa-2-azadiene, reacting with cyclohexadiene to afford the nitronic ester **5** in 19% yield and also serves as a 1-oxadiene forming the enol ether **6** in 20% yield. The similar yields of the four products suggest energetically similar competitive pathways.

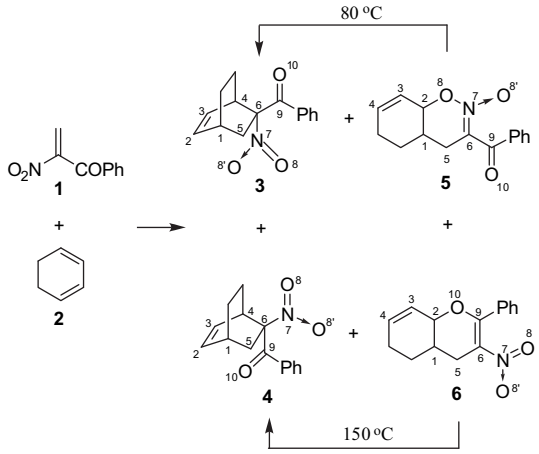

Scheme 1.

The zwitterion **7** was proposed as a possible common intermediate on the pathways leading to nitronic ester **5** and enol ether **6**. Such a zwitterion has precedence in the $SnCl_4$-catalyzed Diels–Alder reaction of 1-nitrocyclohexene with cyclopentene.[2]

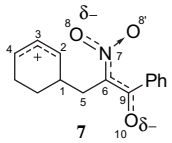

Upon heating to 80 °C, the nitronic ester **5** underwent a [3,3]-sigmatropic rearrangement to give exclusively the bridged bicyclic nitroketone **3**. Conversely, enol ether **6** underwent [3,3]-sigmatropic rearrangement (Claisen rearrangement) upon heating to 150 °C to yield exclusively the isomeric nitroketone **4**. The presence of zwitterion **7** in these rearrangements was considered, but clearly a single zwitterion cannot explain the formation of separate products. The present theoretical study was undertaken to further

* Corresponding authors. Tel.: +1 718 368 5756; fax: +1 718 368 4876 (H.X.); tel.: +1 215 895 2652; fax: +1 215 895 1265 (P.A.W.); *e-mail addresses:* hxu@kingsborough.edu (H. Xu), wadepa@drexel.edu (P.A. Wade).

0040-4020/$ – see front matter © 2009 Elsevier Ltd. All rights reserved.
doi:10.1016/j.tet.2009.11.075

investigate the reaction mechanisms involved in these cycloadditions and subsequent rearrangements.

2. Computational methods

All structures were fully optimized at the B3-LYP[3,4] level using the 6-311G(d)[5] basis set. The reliability of the B3-LYP method has been demonstrated for application to Diels–Alder reactions and pericyclic reactions.[6–9] In addition, the B3-LYP/6-311G(d) level of theory generally yields satisfactory structures and energies for N-containing compounds.[10] Vibrational frequencies were computed for all geometries at the same computational level, mainly to characterize the species as either local minima or transition states. For each transition state, an IRC (intrinsic reaction coordinate) computation was carried out to locate the two structures connected by the transition state. Since each reaction under study was carried out in solution, once the potential energy surface (PES) was mapped out at the B3-LYP/6-311G(d) level, solvent correction was performed by means of PCM (polarizable continuum model) calculations using the Gaussian03 suite of programs. A mixed solvent composed of equal amounts of benzene and dichloromethane was employed in the cycloaddition reaction of nitroketone **1** with cyclohexadiene.[1] Since solvent mixture parameters are not available in Gaussian03, the PCM calculations were performed using published parameters for dichloromethane, the more polar solvent component. The [3,3]-sigmatropic rearrangement of **5** to produce **3** was carried out in 95% ethanol,[1] so ethanol was used for the PCM correction. For the rearrangement of **6** to **4**, DMF was the solvent.[1] Parameters for DMF are not available in PCM of Gaussian03. DMSO has a somewhat higher dipole moment and dielectric constant than DMF but is the closest alternative with available parameters: DMSO parameters were accordingly used for the PCM correction. All PCM corrections were obtained by single-point computations on the B3-LYP/6-311G(d)-optimized structures. Zero-point energy (ZPE) corrections were applied to determine relative stabilities.

For computations at the B3-LYP/6-311G(d) level, all energies are reported as total energies in kcal/mol unless otherwise specified, and all interatomic distances are in Angstroms (Å). All computations were performed using the Gaussian03[11] suite of programs on the IBM p690 (Teragrid) and SGI Altix (Teragrid) computers available at the National Center for Supercomputing Applications (NCSA). The vibrations corresponding to the vibrational frequencies computed at the B3-LYP/6-311G(d) level were visualized using HyperChem[12] for PC.

3. Results

The cycloaddition pathways were modeled according to the mode of involvement of the nitroketone **1** in its reaction with cyclohexadiene. The nitroketone **1** functions as a dienophile activated by two electron-withdrawing groups (the geminal nitro and carbonyl groups) in the two pathways investigated for the formation of **3** and **4**. Nitroketone **1** also functions as a heterodiene, either as C=C–N=O or as C=C–C=O, in the other two reaction pathways leading to **5** and **6**, respectively. The atomic numbering used for discussion is shown in Scheme 1. Because the reactions studied here were carried out using different solvents, the PCM corrected energies should be more accurate and are, indeed, in better agreement with experimental observations. Therefore, the energies referred to in the sections below include PCM corrections unless otherwise stated.

3.1. Formation of cycloadducts 3 and 5

Study of the pathway leading to formation of nitroketone **3** was attempted first. Only the transition state **8** (Fig. 1) was found using the Cartesian coordinates for reactants **1**–**2** and product **3**. However, the IRC computation of the transition state **8** clearly places it on the pathway from reactants to the nitronic ester **5** instead of the nitroketone **3**. The activation energy is 12.6 kcal/mol and product **5** is 12.3 kcal/mol more stable than the reactants (Fig. 2). The reaction to produce nitronic ester **5** is concerted: there is no indication of a zwitterion intermediate. Tens of trials were performed, all of which consistently pointed to the transition state **8** on the pathway to nitronic ester **5**. No pathway on the potential energy surface starting from the reactants leading to nitroketone **3** could be found by IRC computation. Although subsequent [3,3]-sigmatropic rearrangement of nitronic ester **5** does yield the nitroketone **3** over several hours at 80 °C, rearrangement does not occur under the lower temperature conditions employed for cycloaddition (50 °C, 1 h).[1] How then, is product **3** produced from the reactants on the PES? Could products **3** and **5** share **8** as a common transition state? In order to answer these questions, the underlying principles of IRC computation were considered and the results depicted in Figure 3 are proposed.

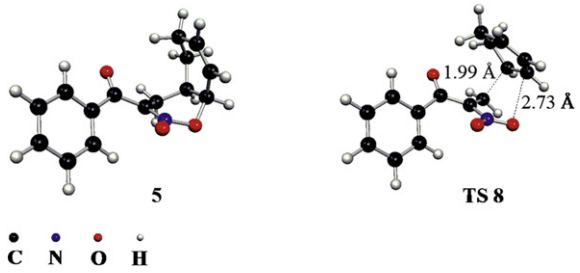

Figure 1. The 3-D structures **5** and **8**.

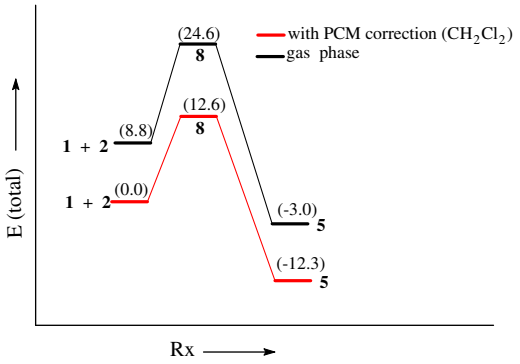

Figure 2. Potential energy profiles (relative energies (kcal/mol, ZPE corrected) are shown in parentheses) for formation of nitronic ester **5**.

The IRC is defined as the steepest descent path connecting reactants, transition state, and product.[13] This is the path with the greatest absolute values of gradients, for example, the intrinsic path IRP (a) in Figure 3. Although there is no IRC computation that can confirm the connection between reactants **1**–**2** and product **3**, it does not mean that no computational path exists. What it does mean is that the steepest descent from reactants leads to nitronic ester **5** and not to product **3**. For example, path (b) is not excluded from the potential energy surface even though it is not the steepest descent path.

It is very common that transition states connect local minima in sequential reactions. Mathematically, such PES can be viewed as two saddle surfaces that smoothly intersect, as shown in Figure 4. Since the saddle surfaces III and IV both curve downward, they can physically intersect without significant distortion. The place where the two surfaces intersect corresponds to a local minimum. In this

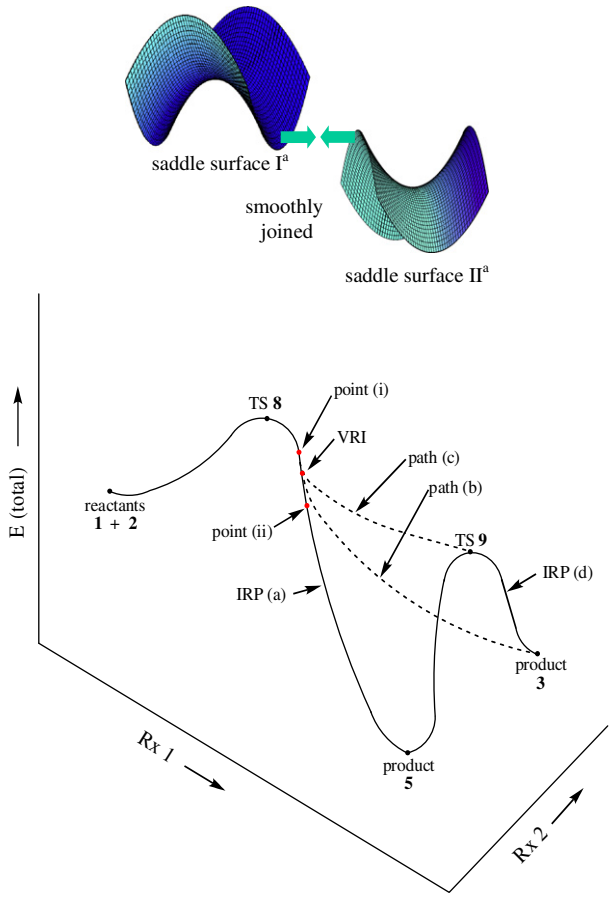

Figure 3. Proposed schematic PES for cycloaddition to and interconversion of nitroketone **3** and nitronic ester **5**. [a]Saddle surfaces were drawn using SurfX3D freeware (version 2.0, 2007, Clark Dailey, Woodbury, MN).

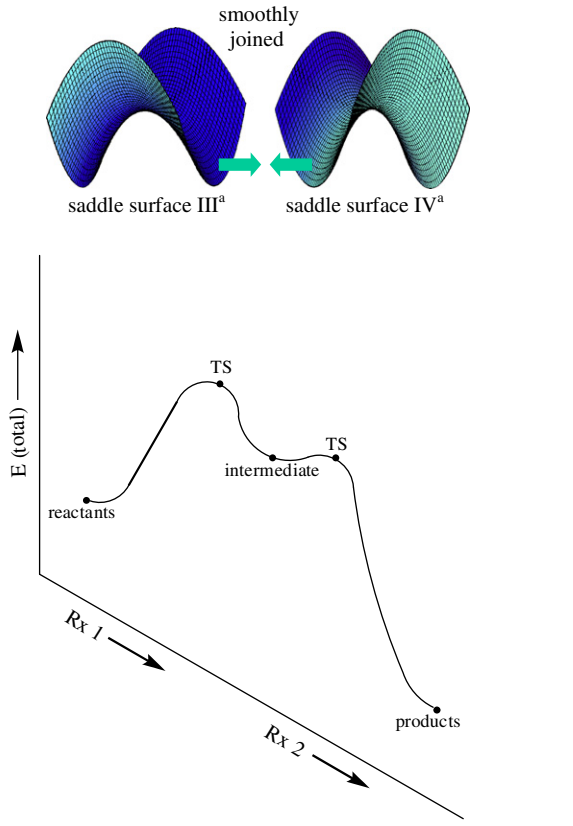

Figure 4. The potential energy profile of a two-step sequential reaction. [a]Saddle surfaces were drawn using SurfX3D freeware (version 2.0, 2007, Clark Dailey, Woodbury, MN).

case, the reaction coordinate of the first step is parallel to that of the second step. Accordingly, the product of the first step becomes the reactant of the second step. Besides the common situation illustrated in Figure 4, in some specific chemical systems,[6,7] a transition state may connect a local minimum and another transition state instead of two local minima. Consider path (c) in Figure 3. Mathematically, this situation can be treated as two saddle surfaces smoothly intersecting in a way different from that illustrated in Figure 4. In Figure 3, the saddle surface I is the same as the saddle surface III in Figure 4. The saddle surface II corresponds to saddle surface IV but has been rotated clockwise by 90° and lowered so that the saddle point lies below the saddle point of surface I. In order to achieve smooth intersection, both surfaces must distort to some extent since they are mismatched (I curves up and II curves down). The distortion necessary for smooth connectivity is a flattening of the two surfaces. Here the two reaction coordinates are orthogonal (i.e., the reaction coordinate 2 is perpendicular to the reaction coordinate 1). The vibrational frequency corresponding to the transformation of product **5** to product **3** is negative in the neighborhood of transition state **9** only along reaction coordinate 2. The IRP (d) illustrates this possibility. The vibrational frequency for transformation of product **5** to product **3** is positive along reaction coordinate 1 over the range from transition state **8** to transition state **9**, path (c). Since the PES involves smooth transition from saddle surface I to surface II, all first and second derivatives are continuous. Consider advancement along reaction coordinate 1 from transition state **8** to transition state **9** on pathway (c). In the neighborhood of **8**, the vibration corresponding to formation of product **3** from product **5** [i.e., perpendicular to the IRP (d)] has a positive vibrational frequency. In the neighborhood of transition state **9**, the vibrational frequency has a negative sign. Mathematically, the vibrational frequency is a second derivative. Since the second derivative is continuous on the potential energy surface, it must become zero at some point between transition states **8** and **9**. This point is the well known valley-ridge inflection point (VRI). A number of chemical systems containing VRI have been documented.[6–9,14–18] Given that the second derivative is zero at the VRI, the curvature is zero since curvature is a function of the second derivative. Thus, the surface is flat near the VRI (along a direction parallel to movement from product **5** to product **3**). A value of zero for the second derivative has an additional consequence. The restoring force is also zero since it is proportional to the vibrational frequency. As a result, it takes no effort to stray from path (c) at the VRI. The pathway bifurcates toward products (either **5** or **3**) or continues as path (c) toward transition state **9**. This bifurcation successfully accounts for why there is no calculable transition state connecting reactants **1**–**2** to product **3**, and why the IRC computation of **8** cannot confirm the existence of **3** as one of two local minima. Many other theoretical studies have established reactions with bifurcation.[6–9,14–18] In particular, the Diels–Alder reaction of nitroethylene and cyclopentadiene has shown a similar bifurcated pathway to the one proposed here.[8]

Since it is postulated that products **3** and **5** form from the common transition state **8**, the relative percentage of products is a result of the branching ratio at the VRI. Here the branching ratio must be nearly 1:1 because within experimental error, the products were formed in equal yield. The branching ratio should depend on reaction dynamics, as is believed to be true for published examples of other reactions with bifurcations.[6–8]

In the present case, the IRC does not connect transition states **8** and **9**. The IRC and the other two trajectories branch at the VRI. Therefore, studying the IRC alone cannot locate the position of the VRI: a rigorous potential energy surface scan would be required.

Given available computational resources, such a PES scan at the B3-LYP/6-311G(d) level starting from **8** is not readily feasible. Fortunately, a point-by-point study along the IRP does provide convincing evidence of the existence of a VRI.

At the VRI, the vibrational frequency corresponding to the transformation of **5** to **3** must be zero. Two points on the IRP near the expected VRI were examined. At point (i), the structure is 1.9 kcal/mol (Table 1) more stable than **8** and the vibrational frequency corresponding to the reaction from **5** to **3** is 54 cm^{-1}, indicating that the potential energy surface around point (i) is very flat. Moreover, point (i) occurs prior to the VRI on the path since the frequency value is positive. Descending to point (ii) along the IRC, the total energy drops 0.4 kcal/mol (Table 1) and the vibrational frequency corresponding to conversion of **5** to **3** becomes −61 cm^{-1}. This small negative number again demonstrates that the surface is very flat around point (ii), and that point (ii) is past the VRI since the value is negative.

Table 1
Total energies relative to TS **8** and vibrational frequencies for molecular arrays on the path from **5** to **3**

Species	Relative energy, kcal/mol	Vibrational frequency (cm^{-1})
TS **8**	0.0	N/A
Point (i)	−1.9	+54
Point (ii)	−2.3	−61
Additional point	−3.1	−83
Additional point	−3.6	−106
Additional point	−4.2	−129
TS **9**[a]	−4.7	−188

[a] TS **9** is included for reference.

The vibrational frequency corresponding to the rearrangement of **5** to **3** changes signs from point (i) to point (ii). Therefore, the VRI must lie in the interval between these points. The 3-D structures at points (i) and (ii) are depicted in Figure 5 and the molecular array at the VRI should be similar to both of these structures.

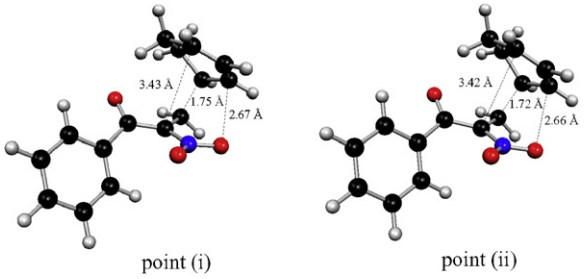

Figure 5. Structures at points (i) and (ii) on the PES for formation of **3** and **5**.

3.2. Formation of cycloadducts 4 and 6

Study of the pathway leading to formation of nitroketone **4** was attempted next. Only transition state **10** (Fig. 6) was found using the Cartesian coordinates of the reactants **1**–**2** and product **4**. The IRC computation of **10** confirms the connection of the reactants and enol ether **6** rather than nitroketone **4** (Fig. 7). A thorough search (tens of trials) was performed for another possible transition state but only the one could be located.

A second bifurcated pathway would explain formation of nitroketone **4** and enol ether **6** (Fig. 8). The energy barrier from the reactants to transition state **10** is 12.7 kcal/mol and the enol ether **6** is 15.5 kcal/mol more stable than the reactants. In particular, this second pathway should compete successfully with the bifurcated pathway affording products **3** and **5**: the calculated ΔE_a is only 0.1 kcal/mol. There is no IRC computation showing a connection

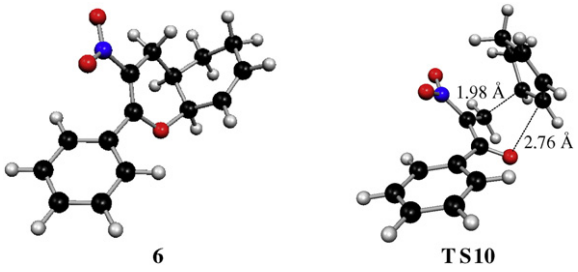

Figure 6. Structures **6** and **10**.

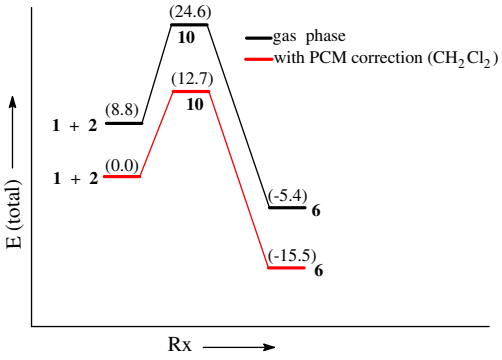

Figure 7. Potential energy profiles (relative energies (kcal/mol, ZPE corrected) are shown in parentheses) for formation of enol ether **6**.

between reactants and **4** at the B3-LYP/6-311G(d) level. This situation is similar to that of the bifurcated pathway to products **3** and **5**. Thus, a second bifurcated pathway appears to be present for the cycloaddition reactions giving products **4** and **6**. Products **4** and **6** are formed from the reactants through the common transition state **10**. Descent from **10** on the IRC follows the bottom of the valley (i.e., the steepest descent) reaching the VRI from where bifurcation occurs. Similar to the bifurcating pathway to products **3** and **5**, reaction may lead to the transition state **11**, or branch off giving products **4** and **6** directly. The IRC computation for transition state **10** results in the pathway to enol ether **6**. Bifurcation explains why no transition state could be located between reactants **1**–**2** and nitroketone **4** and why the IRC leads to **6** rather than **4**: the path from **10** to **4** does *not* have the steepest descent.

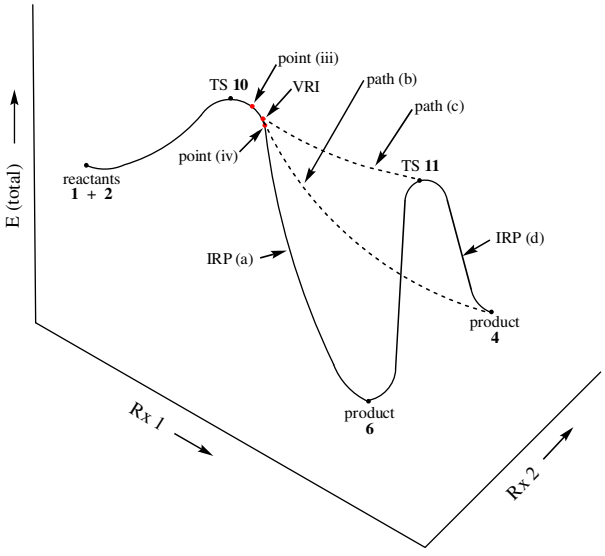

Figure 8. Proposed schematic PES for cycloaddition to and interconversion of nitroketone **4** and nitronic ester **6**.

In the formation of products **4** and **6**, the branching ratio must be nearly 1:1 because within experimental error, the products were formed in equal yield. This situation parallels observations for the formation of products **3** and **5** in the first bifurcated pathway.

Convincing evidence for the VRI in Figure 8 was obtained by performing a point-by-point computation of the IRC. At point (iii), the structure is 2.48 kcal/mol more stable than **10** (Table 2). The 3-D structure at point (iii) is shown in Figure 9. Its vibrational frequency on the conversion pathway from **6** to **4** is 65 cm^{-1}. Point (iii) occurs prior to the VRI since this value is positive. Descending to point (iv), which is 2.54 kcal/mol more stable than **10** (ΔE from point (iii) is only 0.06 kcal/mol), the vibration corresponding to conversion of **6** to **4** has the imaginary frequency of −4 cm^{-1} and must be just past the VRI. Such small positive and negative frequency values again indicate a flat PES in this region. The VRI for conversion of reactants **1**–**2** to products **4** and **6** must lie between points (iii) and (iv) along the IRC from transition state **10** to enol ether **6**. The molecular array at the VRI must be very close to the structure shown for point (iv), which had a nearly zero vibrational frequency.

Table 2
Total energies relative to TS **10** and vibrational frequencies for molecular arrays on the path from **6** to **4**

Species	Relative energy, kcal/mol	Vibrational frequency (cm^{-1})
TS **10**	0.0	N/A
Point (iii)	−2.48	+65
Point (iv)	−2.54	−4
Additional point	−2.6	−8
Additional point	−2.7	−18
Additional point	−3.0	−28
Additional point	−3.2	−39
Additional point	−3.5	−52
Additional point	−3.7	−69
Additional point	−3.84	−76
TS **11**[a]	−3.83	−152

[a] TS **11** is included for reference.

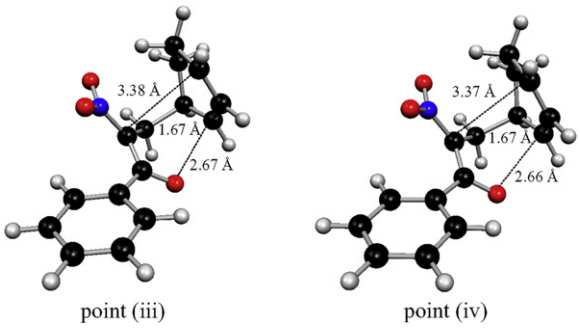

Figure 9. Structures at points (iii) and (iv) on the PES for formation of **4** and **6**.

3.3. *O*-Allyl nitronic ester rearrangement of 5 to 3

The fully optimized structures for nitronic ester **5** and nitroketone **3** are shown in Figures 1 and 10, respectively, and energies are listed in Table 3. Rearrangement of **5** occurs via a pathway exhibiting the single transition state **9** with an E_a of 20.4 kcal/mol after the PCM correction (Fig. 11). The nitroketone **3** is 5.3 kcal/mol more stable than the nitronic ester **5** and E_a for the reverse reaction is 25.7 kcal/mol. From the computational data, it appears that rearrangement of **5** is both thermodynamically and kinetically irreversible under the reaction conditions (80 °C). The stereochemical outcome of the rearrangement is dictated by the structure of the transition state **9** where the nitro group must have *endo* orientation. As was experimentally observed, **5** gave exclusively the nitroketone **3** with an *endo*-nitro group and none of the isomeric nitroketone **4**.

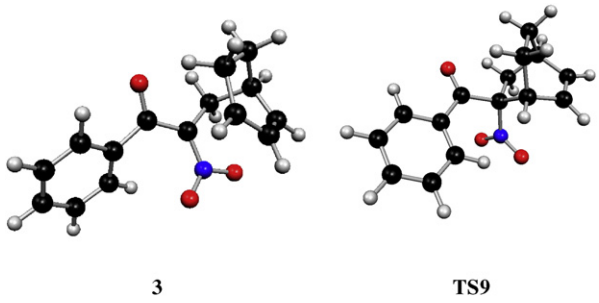

Figure 10. Structures **3** and **9**.

Table 3
Relative energy for calculated structures on the rearrangement pathways

Species	Pathway	In gas phase, kcal/mol	PCM corrected, kcal/mol
5	**5** to **3**	10.6	0.0
TS 9	**5** to **3**	34.9	20.4
3	**5** to **3**	3.3	−5.3
6	**6** to **4**	12.0	0.0
TS 11	**6** to **4**	39.5	25.1
4	**6** to **4**	5.2	−3.9

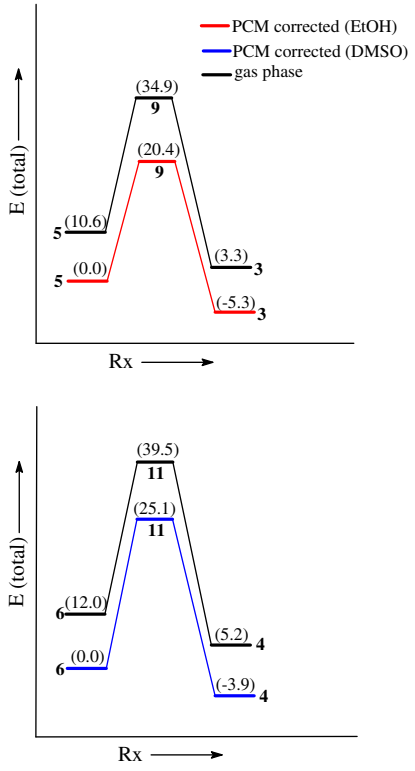

Figure 11. Potential energy profiles (relative energies (kcal/mol, ZPE corrected) are shown in parentheses) for the sigmatropic rearrangements of nitronic ester **5** and enol ether **6**.

In ethanol, transition state **9** experiences more stabilization than the reactant, nitronic ester **5**. This indicates that polar solvents should speed up the [3,3]-sigmatropic rearrangement of **5**. This has

not been studied experimentally for nitronic ester **5**. The related rearrangement of *O*-allyl nitronic ester **12** did, however, proceed more rapidly in ethanol than in benzene.[1]

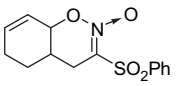

12

3.4. Claisen rearrangement of 6 to 4

Optimized structures for enol ether **6** and nitroketone **4** are shown in Figures 6 and 12, respectively. A single transition state, structure **11**, is found on the reaction pathway and E_a is 25.1 kcal/mol after the PCM correction (Fig. 11 and Table 3), consistent with the relatively high temperature (150 °C) needed for rearrangement. The nitroketone **4** is 3.9 kcal/mol more stable than enol ether **6**. Thus, the rearrangement of **6** would be very slow and essentially irreversible under the reaction conditions (150 °C). The stereochemical outcome is determined by the structure of the transition state **11** in which the nitro group must be located *exo*. This is fully consistent with the experimental result where only nitroketone **4** is formed and none of the isomeric nitroketone **3**.[1]

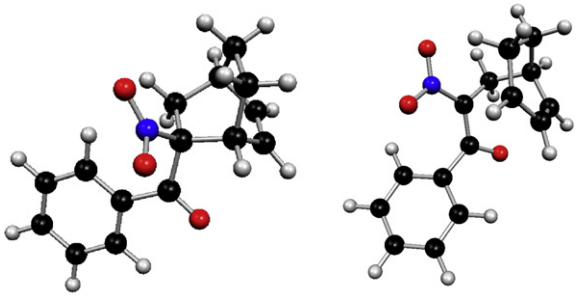

4 **TS11**

Figure 12. Structures **4** and **11**.

4. Discussion and conclusions

Although the bifurcated formation of **3** and **5** has the common transition state **8**, nitroketone **3** is 5.3 kcal/mol more stable than nitronic ester **5**. Accordingly, the branching ratio for formation of **3** and **5** should be close to 1:1 only if the cycloaddition reactions are under kinetic control. Conversely, the nitroketone **3** would be expected to heavily predominate over the nitronic ester **5** if the reactions were thermodynamically controlled. Experimentally, **3** and **5** are obtained in essentially equal yield.[1] It can then be concluded that cycloaddition to produce **3** and **5** is under kinetic control. A similar situation prevails in the cycloaddition leading to **4** and **6**, which share transition state **10** and where compound **4** is 3.9 kcal/mol more stable than **6**. Here, too, the experimental product ratio is 1:1 and therefore reaction must be kinetically controlled.

From the bond distances in cycloaddition transition state **8** (C_1–C_5, 1.99 Å; C_2–O_8, 2.73 Å) it is clear that bond development is concerted but highly asynchronous. At point (i) near the VRI, the C_2–O_8 distance is 2.67 Å and further approach of these atoms would occur as nitronic ester **5** forms. Conversely, the C_4–C_6 distance is 3.43 Å and further approach of these atoms would occur as nitroketone **3** forms. The bond distances in transition state **10** [C_1–C_5, 1.98 Å; C_2–O_{10} 2.76 Å (Fig. 6)] indicate that this reaction is also concerted but asynchronous. At point (iii) near the VRI, the C_2–O_{10} distance is 2.67 Å and further approach of these atoms would occur as enol ether **6** forms. The incipient C_4–C_6 bond distance of nitroketone **4** is 3.38 Å at point (iii).

Although the IRC does not connect reactants **1**–**2** to transition state **9**, the steepest descent path from **8** is believed to pass relatively close to transition state **9**. The vibrational frequencies for additional points corresponding to rearrangement of **5** approach that of **9** ($-188\ cm^{-1}$) during the descent from **8** along the IRC (Table 1). Similarly, the vibrational frequencies for additional points corresponding to the Claisen rearrangement of enol ether **6** (Table 2) begin to approach that of transition state **11** ($-152\ cm^{-1}$) during the descent from **10** along the IRC. Even though the IRC computation does not confirm the connection of **1**–**2** and **11**, the steepest descent from **10** appears to pass relatively close to **11**.

Since the cycloaddition reaction producing compounds **3**–**6** was carried out in dichloromethane/benzene, comparison of the relative stabilities in dichloromethane should be more appropriate than comparison in the gas phase. In dichloromethane, the relative stabilities from most to least stable are in the following order: **4**>**3**>**6**>**5**. See Figure 13 for relative energies. In summary, **4** is 1.8 kcal/mol more stable than **3** in dichloromethane, **3** is 2.6 kcal/mol more stable than **6**, and **6** is 2.9 kcal/mol more stable than **5**. If the pathway interconnecting **3** and **5** were thermodynamically reversible, then **3** would heavily predominate, and the amount of **5** formed would be negligible. Likewise, if the pathway interconnecting **4** and **6** were thermodynamically reversible, then **4** would heavily predominate. Because these results were *not* the case experimentally, the reactions must have been thermodynamically irreversible under the cycloaddition conditions. The cycloaddition pathways leading to **3**–**6** are then kinetically controlled based on the experimental data and from the relative stabilities of products **3**–**6**.

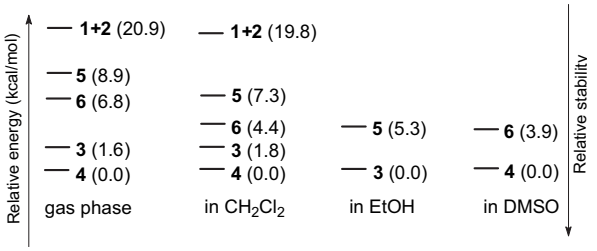

Figure 13. Relative energies (shown in parentheses (kcal/mol, ZPE corrected)) of **3**–**6** in the gas phase and after PCM correction.

In ethanol, the nitroketone **3** is 5.3 kcal/mol more stable than the nitronic ester **5** (Fig. 13) despite the strain inherent in a bicyclo[2.2.2]oct-2-ene ring system. The activation energy for rearrangement is 20.4 kcal/mol (Fig. 11), which is in agreement with the observation that **5** is converted to **3** at 80 °C in 95% ethanol over 3 h.[1] This new reaction would appear to be thermodynamically controlled as is the common case in sigmatropic rearrangements.

The nitroketone **4** is 3.9 kcal/mol more stable than the enol ether **6** in DMSO and the activation energy for rearrangement is 25.1 kcal/mol, higher than that for rearrangement of nitronic ester **5**. These data are again consistent with the experimental observations: rearrangement of **6** afforded **4** in DMF only at 150 °C over 42 h. Rearrangement of **6** required significantly higher temperature and longer reaction time than rearrangement of nitronic ester **5**.

With PCM corrections, the potential energy profiles of the competing Diels–Alder reactions and the relative stabilities of **3**–**6** successfully account for the experimental yields of the cycloaddition products. The computational data for the sigmatropic rearrangements of **5** and **6** are also in very good agreement with the experimental results. Moreover, no evidence was found for the presence of zwitterionic intermediates in any of the reactions. This is in marked contrast to the rearrangement of nitronic esters in the presence of tin(IV) chloride.[19]

Finally, it should be noted that the *O*-allyl nitronic ester rearrangement appears to have a highly favorable driving force. The rearrangement of nitronic ester **5** is more energetically favorable than the corresponding Claisen rearrangement of enol ether **6** by 1.4 kcal/mol. Although this difference is small and possibly within computational error, it provides an incentive to pursue additional *O*-allyl nitronic ester rearrangements. These rearrangements are apparently more energetically favorable than the related Claisen rearrangements.

Acknowledgements

This project was partially supported by the National Center for Supercomputing Applications (NCSA) under Grant Numbers CHE060061N, CHE060062, and CHE090067, and utilized the IBM p690 (Teragrid) and SGI Altix (Teragrid) available at NCSA. Computing time was partly provided by the Mississippi Center for Supercomputing Research (MCSR). Technical support was generously provided by Dr. B.W. Hopkins of MCSR.

Supplementary data

Supplementary data associated with this article can be found in the online version at doi:10.1016/j.tet.2009.11.075.

References and notes

1. Wade, P. A.; Murray, J. K., Jr.; Shah-Patel, S.; Le, H. T. *Chem. Commun.* **2002**, 1090–1091.
2. Denmark, S. E.; Cramer, C. J.; Sternberg, J. A. *Helv. Chim. Acta* **1986**, *69*, 1971–1989.
3. Becke, A. D. *J. Chem. Phys.* **1993**, *98*, 1372–1377.
4. Lee, C.; Yang, W.; Parr, R. G. *Phys. Rev. B* **1988**, *37*, 785–789.
5. Krishnan, R.; Binkley, J. S.; Seeger, R.; Pople, J. A. *J. Chem. Phys.* **1980**, *72*, 650–654.
6. Zhou, C.; Birney, D. M. *Org. Lett.* **2002**, *4*, 3279–3282 and references therein.
7. Ess, D. H.; Wheeler, S. E.; Iafe, R. G.; Xu, L.; Celebi-Olcum, N.; Houk, K. N. *Angew. Chem., Int. Ed.* **2008**, *47*, 7592–7601 and references therein.
8. Celebi-Olcum, N.; Ess, D. H.; Aviyente, V.; Houk, K. N. *J. Org. Chem.* **2008**, *73*, 7472–7480 and references therein.
9. Celebi-Olcum, N.; Ess, D. H.; Aviyente, V.; Houk, K. N. *J. Am. Chem. Soc.* **2007**, *129*, 4528–4529.
10. Dobbs, K. D.; Sohlberg, K. *J. Chem. Theory Comput.* **2006**, *2*, 1530–1537.
11. Frisch, M. J.; Trucks, G. W.; Schlegel, H. B.; Scuseria, G. E.; Robb, M. A.; Cheeseman, J. R.; Montgomery, J. A., Jr.; Vreven, T.; Kudin, K. N.; Burant, J. C.; Millam, J. M.; Iyengar, S. S.; Tomasi, J.; Barone, V.; Mennucci, B.; Cossi, M.; Scalmani, G.; Rega, N.; Petersson, G. A.; Nakatsuji, H.; Hada, M.; Ehara, M.; Toyota, K.; Fukuda, R.; Hasegawa, J.; Ishida, M.; Nakajima, T.; Honda, Y.; Kitao, O.; Nakai, H.; Klene, M.; Li, X.; Knox, J. E.; Hratchian, H. P.; Cross, J. B.; Bakken, V.; Adamo, C.; Jaramillo, J.; Gomperts, R.; Stratmann, R. E.; Yazyev, O.; Austin, A. J.; Cammi, R.; Pomelli, C.; Ochterski, J. W.; Ayala, P. Y.; Morokuma, K.; Voth, G. A.; Salvador, P.; Dannenberg, J. J.; Zakrzewski, V. G.; Dapprich, S.; Daniels, A. D.; Strain, M. C.; Farkas, O.; Malick, D. K.; Rabuck, A. D.; Raghavachari, K.; Foresman, J. B.; Ortiz, J. V.; Cui, Q.; Baboul, A. G.; Clifford, S.; Cioslowski, J.; Stefanov, B. B.; Liu, G.; Liashenko, A.; Piskorz, P.; Komaromi, I.; Martin, R. L.; Fox, D. J.; Keith, T.; Al-Laham, M. A.; Peng, C. Y.; Nanayakkara, A.; Challacombe, M.; Gill, P. M. W.; Johnson, B.; Chen, W.; Wong, M. W.; Gonzalez, C.; Pople, J. A. *Gaussian 03, Revision D.01*; Gaussian: Wallingford, CT, 2004.
12. *HyperChem 6.03 Version for Windows*; HyperCube: Gainesville, FL, 2000.
13. Levine, I. N. *Quantum Chemistry*, 4th ed.; Prentice-Hall: Upper Saddle River, NJ, 1991, Chapter 15, p 540 and reference therein.
14. Schlegel, H. B. In *Encyclopedia of Computational Chemistry*; Schleyer, P. v. R., Ed.; Wiley: New York, NY, 1998; Vol. 4, pp 2432–2437; Kraka, E. In *Encyclopedia of Computational Chemistry*; Schleyer, P. v. R., Ed.; Wiley: New York, NY, 1998; Vol. 4, p 2445.
15. Gonzalez, C.; Schlegel, H. B. *J. Chem. Phys.* **1989**, *90*, 2154–2161.
16. Gonzalez, C.; Schlegel, H. B. *J. Phys. Chem.* **1990**, *94*, 5523–5527.
17. Taketsugu, T.; Tajima, N.; Hirao, K. *J. Chem. Phys.* **1996**, *105*, 1933–1939.
18. Taketsugu, T.; Kumeda, Y. *J. Chem. Phys.* **2001**, *114*, 6973–6982.
19. Wade, P. A.; Pipic, A.; Santhanaraman, M.; Le, H. T. *Chem. Commun.* **2009**, 3531–3532.